Modelling of water infiltration and soil swelling in a vertisol from Guadeloupe

Stephane Ruy, Yves-Marie Cabidoche, Liliana Di Pietro

Modelling of water infiltration and soil swelling in a vertisol from Guadeloupe

S. Ruy[1,*], Y.M. Cabidoche[2] and L. Di Pietro[3]

[1] and [3]: INRA - Science du Sol; Domaine St Paul; Agroparc; 84914 Avignon Cedex 9; FRANCE. [2]: INRA - AgroPédoClimatologie; Domaine Duclos; Prise d'Eau; 97140 Petit-Bourg; French West Indies.

Email: [1] ruy@avignon.inra.fr; [2]: cabidoch@antilles.inra.fr; [3]: lili@avignon.inra.fr

[*]: corresponding author.

MS-No: HSA6.4-0007

Abstract

Models of water infiltration in undisturbed swelling soils rely on a dual porosity concept: Darcy flow in the micro (matric) porosity and by-pass flow in cracks. In vertisols a third component must be added: the structural porosity, excluding cracks, formed by the soil microfauna activity and containing water easily available for plants. A model was implemented to study the mechanisms of water infiltration: (i) water infiltration in the matric porosity is modelled by the Darcy's law, (ii) the flow in the structural porosity is a gravity-dominated flow, (iii) water entering cracks is instantaneously added at the bottom of the cracks. Water movements from structural to matric porosity and from crack's wall into soil matrix are accounted for. Cracks' opening is a function of soil matrix moisture. Shrinkage curve, retention curve and hydraulic conductivity of the matrix were measured in the laboratory. The anisotropy ratio of soil deformation was measured *in situ*. Experiments were conducted *in situ* to fit some soil structure parameters and test the model. Although not wholly validated because of a poor modelling of infiltration in structural porosity, the model already shows that infiltration in this soil is a 3D process and that water infiltration in structural porosity is the main factor of rainfall partition between vertical infiltration in the soil matrix and water flow into the cracks.

1- Introduction

A model of infiltration and soil deformation in a Vertisol should account for three porosity compartments (Cabidoche & Ozier-Lafontaine, 1995; Ruy, 1997): macro-cracks delimiting continuous soil prisms, intra-prism structural porosity and matric porosity. The almost vertical macro-cracks, several centimetres wide and several decimetres apart, open and close as the clay particles reorganise in response to soil moisture changes. Water entering these cracks may infiltrate laterally into the walls of the soil matrix. The matric porosity is formed by the arrangement of clay particles. Matric pores are less than 5 µm in width. They remain saturated during structural and normal shrinkage and thus contain the water responsible for soil movement. The limit between structural and normal shrinkage is called the crack air entry (CAE) point. The intra-prism structural porosity has a relatively stable geometry (Cabidoche & Ozier-Lafontaine, 1995). Structural pores are from 10 µm to several mm in width (Ruy, 1997). Structural water does not induce any deformation of the soil. Shrinkage cracks are not included in structural porosity.

In order to better understanding the processes of water infiltration in an undisturbed swelling clay soil, we present the physical bases of a 2D numerical model of water infiltration and soil movements in a Vertisol.

2- Physical bases and description of the model

The model is 2D, the scale of modelling is a half prism isolated by one macro-crack. The experimental size of a prism can be deduced from the network of macro-cracks and is about 70 cm.

(i) water flow in the matric porosity

We assume that water flow is described by Darcy's law because of the small diameter and the homogeneous distribution of the size of the matric pores (Ruy, 1997). 2D Richard's equation is used to calculate water fluxes. A source function S_{w} accounts for the diffusive water movement from structural porosity to matric porosity, as suggested by Jarvis (1994):

$$S_w = K_{w/s}\left(\psi_{\mathrm{mat}}\right) \cdot S_{\mathrm{struc}} \cdot \frac{\psi_{\mathrm{struc}} - \psi_{\mathrm{mat}}}{d^2} \quad , \tag{1}$$

where $K_{\mathrm{w/s}}$ (cm s^{-1}) is the matric conductivity, ψ_{mat} (cm) the potential of water in matric porosity, ψ_{struc} (cm) the potential of water in structural porosity, S_{struc} the saturation of structural porosity and d (cm) an effective "diffusion" length. We suppose that the potential of water in the structural porosity is a linear function of the saturation of this porosity: ψ_{struc} is equal to 0 cm when the structural porosity is saturated and is equal to ψ_{ae} when it is air filled, where ψ_{ae} is the soil water potential at the CAE point (Ruy, 1997). The water retention curve, the shrinkage curve and the matric hydraulic conductivity were measured according to the methods described in Ruy & Cabidoche (1998).

We used the finite element method to discretize the domain with rectangular elements. The boundary condition at the surface is a Neumann's condition according to *(iv)*. A zero flux condition is imposed at the bottom of the profile and along the vertical axis of the soil prism, because of the symmetry of the soil prism. The boundary condition along the macro-crack wall is a function of the depth of ponded water in the crack and is described in subsection *(iii)*.

(ii) water flow in the intra-prism structural porosity

Previous work (Ruy, 1997) showed that water flow inside the prism could not be modelled by Darcy's law with a bimodal hydraulic conductivity and water retention curve, and therefore that water flow inside the structural porosity was of "preferential flow type". Then ,we assume that water flow in the structural porosity is a gravity flow. Water flow is described in a conceptual way by using a model of reservoirs in cascade (one reservoir per layer). For each layer, the volume of the reservoir is the volume of the structural porosity. The output flux q of each reservoir (Figure 1) is a power function of the saturation of the reservoir:

$$q = c \cdot S_{\mathrm{struc}}^{b} \quad , \qquad (2)$$

where c (cm s^{-1}) is the unknown hydraulic conductance, S_{struc} the saturation of the reservoir (*i.e.* the saturation of the structural porosity) and b an empirical exponent. Theoretical values of b can be calculated from the laminar film flow theory in a single, smooth and vertical macropore. For open channel flow, a power law function similar at eq. (2) relates the flow and the depth of water. The value of the exponent depends on the Reynold's number (Chen & Wagenet, 1992). The flow is assumed to be turbulent, and we set the value of b to 1.5.

(iii) water flow into the macro-cracks

In the model, water infiltrating into the macro-crack instantaneously reaches the bottom of the crack where it accumulates. Horizontal infiltration into the soil prism during downward unsaturated flow along the macro-crack wall is neglected, whereas it is taken into account for ponded conditions at the bottom of the macro-crack. Hence, the lateral boundary condition for the resolution of the 2D Richard's equation is a zero flux condition above the surface of the ponded water, and a Dirichlet's condition below this surface (hydrostatic profile). At each time step, the model recalculates the volume of the macro-crack and the depth of the surface of the ponded water according to a mass balance and to the deformation of the soil matrix.

(iv) partitioning of rainfall at the soil surface

Rainfall, R, is partitioned at the soil surface according to the infiltrability of the three porosities: first, *R* enters the matric porosity, then excess water flows into the structural porosity and then into the macro-cracks. The model calculates infiltrability of the three porosities.

(v) deformation of the soil matrix

Clay particles reorganise as water infiltrates into matric porosity, and the soil prism is deformed in every direction according to the anisotropy ratio of soil movements. Swelling is supposed to be normal. We used in the model the anisotropy ratio *k* of Voltz & Cabidoche (1995): *k* is the elongation rate in any horizontal direction divided by the elongation rate in the vertical direction. The model deforms each finite element at each time step according to the variation of the mean matric WC of the element.

Table 1 presents a synthesis of all the equations used in the model.

3- Material and methods

3.1- Description of the experiments

The model was tested on a Vertisol at the Experimental Research Station of INRA in Gardel, Guadeloupe (French Antilles).The soil is a chromic vertisol, with more than 80 % clay.

Several soil prisms were isolated from the plot by a polyethylene sheet coated with a hull of resin and fibreglass. A side of the hull was replaced by a rigid inox steel-plate on which the measurement devices were fixed. Four windows were cut into the inox sheet and equipped with Plexiglas plates. Potentiometric sensors were fitted on the remaining Plexiglas windows to measure the horizontal deformation of a soil prism at different depths. All the displacement sensors were installed on the same soil prism. Thickness variations of prism layers were measured with modified THERESA® transducers (Cabidoche & Ozier-Lafontaine, 1995). Transducers were fitted with the same potentiometric displacement sensors. Water was applied at the soil surface with four full cone nozzles or with a portable sprayer for low intensities.

The matric WC was calculated with the model of Voltz & Cabidoche (1995) from thickness variations of prism layers. The structural WC was not measured. A piezometer was fitted into a macro-crack: an ultrasonic probe automatically measured the level of ponded water.

3.2- Fitting of unknowns parameters

Structural conductance c and diffusion length d must be fitted from experimental data. Both parameters are soil structure parameters: they should vary with depth because the volume and the shape of the structural pores vary with depth. We considered two different values for c: c_{surf} (layers 0-10 cm and 10-30 cm) and c_{deep} (30-50 cm to 90-110 cm). c is nil at 130 cm, because of the impervious layer. Three different values were considered for d: d_{surf} (0-10 cm, 10-30 cm, 30-50 cm), d_{mid} (50-70 cm, 70-90 cm) and d_{deep} (90-110 cm and 110-130 cm). Therefore 5 parameters must be fitted from experiments. We used the Marquardt's method (1963). Six experiments were conducted. The first (Exp1 to Exp5) five were used to calibrate the model, the last one (Exp6) was used to "validate" the model.

4- Results and Discussion

4.1- Submodels validation

The model has been checked against experimental data obtained in a 1D swelling bentonite paste (Angulo, 1989; Figure 1). Then, we used the model in two domains (matric porosity and macro-cracks). A rainfall of 120 mm h^{-1} for 6 min was simulated (frequency 0.9 $year^{-1}$ in the

Grande-Terre Island of Guadeloupe). Figure 2 shows that most of the rain flows into the macro-crack where it accumulates and then infiltrates into the soil prism, resulting in both horizontal and vertical swelling of the prism. The pattern of the heterogeneity of water potentials inside the prism is very similar to the spatial variability of the water content measured in the field (Jaillard & Cabidoche, 1984). Therefore, we consider that these quantitative and qualitative results validate the model when run with 1 or 2 domains.

4.2- Experiments results

Macro-crack flow has never been observed, except in the last experiment. For each experiment, the variation in the swelling measured by transducers is quite large, which is due to a high spatial variability of the structural porosity. During the last experiment, the swelling velocity of a given soil layer increases as the level of water into the macro-crack reaches this layer. It shows that lateral infiltration into the prism of water running rapidly downwards along cracks has to be neglected and that it must be taken into account under the level of ponded water into the macro-crack. Figure 3 shows the relation between the horizontal elongation rate and the vertical one: the slope of the regression line is the anisotropy ratio k. The mean value of k is 0.798 in layer 10-30 cm depth and is 1.152 in layer 30-50 cm depth. It is in agreement with the value of 0.85 calculated by Cabidoche & Voltz (1995). We used a single value of 0.826 for all layers in the model.

4.3- Calibration

For each experiment, the uniqueness of the parameters has been verified (Ruy, 1997). Measured and simulated swelling of 30-50 cm depth soil layer during Exp3 is plotted on Figure 4. For each experiment, a unique set of parameters can be fitted to well simulate the vertical swelling of all soil layers. However, the fitted parameters differ significantly from one experiment to the other: for instance the fitted value (with the 95 % CI) of d_{surf} was 0.28 cm (± 0.01) for Exp2, 0.52 cm (± 0.03) for Exp3, 0.29 cm (± 0.04) for Exp4 and 0.44 cm (±

0.01) for Exp5. As the size of aggregates is a function of the matric WC, we tried to relate d_{surf} to the initial matric WC of the 10-30 cm layer, but the regression was not significant. Fitted values of c_{surf} and c_{deep} also differ from one experiment to another. They can be explained neither by the initial matric WC, nor by rainfall intensity R.

4.4- Validation

Finally, we tested the model with the independent data set collected during Exp6. Parameter values used in the simulation are the mean value that were fitted for Exp1 to Exp5: 0.440 cm for d_{surf}, 2.45 cm for d_{mid}, 2.62 cm for d_{deep}, 0.0434 cm s^{-1} for c_{surf} and 0.0478 cm s^{-1} for c_{deep}. Values of c_{surf} and c_{deep} are those fitted in Exp5 because rainfall intensities of Exp5 and Exp6 are close. Results are presented in Figures 5a and 5b. Neither the range of swelling nor its rate are simulated in a satisfactory way. The beginning of water infiltration into the macro-crack is delayed by the model, because of the high infiltrability of the structural porosity (structural conductance of 0.0434 cm s^{-1} at the surface). However, the upraising of the water level is well simulated. After rainfall has stopped, the decrease of the water level in the macro-crack is not well simulated. However, at least two reasons can explain this discrepancy. (i) clogging of the piezometer by deposit of clay particles: therefore, the level recorded inside the piezometer is higher than the water level in the macro-crack; (ii) artefacts of simulation: as the macro-crack closes up, a small variation in the amount of water in the macro-crack results in a large variation in the level of water.

5. Discussion and conclusion

Germann & Di Pietro (1996) distinguished two kinds of flow in macropores, *i.e.* dispersive and preferential flow. They showed (see Table 3 of Germann & Di Pietro, 1996) that conductance is constant when water infiltration is governed by preferential flow (for large input rates of water), and increases with the rainfall intensity when the flow in macropores is dispersive (for low input rates). In our experiments, low input rates of water in Exp2, Exp3 and at the beginning of Exp4 could be responsible for a dispersive infiltration, whereas the second part of Exp4 and Exp5 could have been governed by preferential flow. However, this result cannot explain the difference between Exp2 and Exp3 where rainfall intensities are the same. In fact, other factors, such as geometry and initial saturation of structural porosity, have an influence upon the value of structural conductance. These authors also showed that gravity-dominated flow could be either of the preferential type or of the dispersive type: in their experiments, the value of *b* was not constant but may be used to assess the degree of preferential flow. *b* decreased with increasing application rates of water. Its value was about 4 for a preferential flow (application rate of water equal to about 360 mm h^{-1}), and increased up to 8 for a more dispersive flow (application rate of about 36 mm h^{-1}). New calibration could be conducted with *b* as an unknown parameter. However, the total number of parameters would increase and parameter *b* and *c* would probably not be independent.

Hypothesis that structural flow is of preferential type came from the results of Ruy (1997). However, the experimental uncertainty in the calculation of structural and matric WC was quite important. It is possible that Darcy's law may apply on one part of the structural flow (in the smallest pores) and that a gravity-dominated flow may be used for the other part of the structural flow, as the range of variation of the pore diameters is quite large. We used the Wind's evaporation method (Tamari *et al.*, 1993) to obtain the hydraulic conductivity of the structural porosity ("structural conductivity") on one saturated clod sampled in the 70-80 cm layer. Results are only approached as the shrinkage is not accounted for in this method, but we see (Figure 6) a good agreement between the matric conductivity and the structural conductivity, showing that Darcy's law could be used at least in one part of the structural porosity.

Nevertheless, the model already shows that water infiltration in a Vertisol is a 3D process and that the structural water flow is the main factor of the partition of rainfall between vertical infiltration in the prism and water flow in macro-cracks, as can be showed in Figures 7a and 7b.

Acknowledgements

We are grateful to MM. J. André, T. Bajazet and A. Mulciba for their technical assistance during the experiments.

References

Angulo-Jaramillo, R., Caractérisation hydrodynamique de sols déformables partiellement saturés. Etude expérimentale à l'aide de la spectrométrie gamma double-sources, PhD. Thesis, Université de Grenoble-INPG, 1989.

Cabidoche, Y.M. and Ozier-Lafontaine, H., THERESA I Matric water content measurements through thickness variations in vertisols. Agricultural Water Management, 28, 133-147, 1995.

Cabidoche, Y.M. and Voltz, M., Non-uniform volume and water content changes in swelling clay soil: II. A field study on a Vertisol. European Journal of Soil Science, 46, 345-355, 1995.

Chen, C. and Wagenet, R.J., Simulation of water and chemicals in macropore soils. Part 1 Representation of the equivalent macropore influence and its effect on soil water flow. Journal of Hydrology, 130, 105-126, 1992.

Germann, P.F. and Di Pietro, L., When is porous media flow preferential? A hydromechanical perspective. Geoderma, 74, 1-21, 1996.

Jaillard, B. and Cabidoche, Y.M., Etude de la dynamique de l'eau dans un sol argileux gonflant: dynamique hydrique. Science du sol, 22, 239-251, 1984.

Jarvis, N.J., The MACRO model (version 3.1): technical description and samples simulations. Reports and Dissertations 19, Swedish University of Agricultural Sciences (Uppsala), 1994.

Ruy, S., Les trois voies simultanées de l'infiltration dans un vertisol de la Guadeloupe: étude expérimentale et numérique. PhD Thesis, University of Montpellier, 1997.

Ruy, S. and Cabidoche, Y.M., Hydraulic conductivity of the matric porosity of an unsaturated Vertisol: a field and laboratory comparison. European Journal of Soil Science, 49, 175-185, 1998.

Voltz, M. and Cabidoche, Y.M., Non-uniform volume and water content changes in swelling clay soil: I. Theoretical analysis. European Journal of Soil Science, 46, 333-343, 1995.

Tamari, S., Bruckler, L., Halbertsma, J. and Chadoeuf, J., A simple method for determining soil hydraulic properties in the laboratory. Soil Science Society of America Journal, 57, 642-651, 1993.

Tables and Figures caption

Tables

Table 1: equations used in the model to described water flow inside and between the three kinds of porosity.

Figures

Figure 1: comparison between the model and experimental data from Angulo (1989) for the profiles of water content during an infiltration in a 1D-swelling bentonite paste.

Figure 2: simulation of water potential distribution inside a prism of a Vertisol during and after rainfall.

Figure 3: relation between the horizontal elongation rate and the vertical one. Only continuous drying periods have been considered, a different number and symbol label each period. The slope of each regression line is the anisotropy ratio *k*. Average values of k are calculated from a weighted mean, the weight being inversely proportional to the estimation variance of *k*.

Figure 4: variation of the measured and simulated swelling of the 30-50 cm depth layer during Exp3. Continuous lines are for the 60 % confidence interval.

Figure 5: simulation of Exp6 with parameters fitted from Exp1 to Exp5. (5a): variation of the measured and simulated swelling of the 10-30 cm depth layer; continuous lines are for the 60 % CI. (5b): variation of the measured and simulated water level in macro-cracks.

Figure 6: hydraulic conductivity $K_{w/s}$ of the matric porosity and of the structural porosity of the 70-80 cm depth layer. θ is the volumetric water content ($m^3\ m^{-3}$).

Figure 7: simulation of: (7a) the cumulated water flow in the three porosities during and after rainfall (I=71 mm h^{-1} for 54 min); and (7b) the cumulated flow in the matric porosity from the soil surface, from the macro-crack and from structural pores

Table 1

porosity	Equations		
	law of motion	mass balance	water exchanges:
matric	Darcy's law : $\mathbf{q}_{\mathrm{mat}} = -K_{\mathrm{w/s}}(\psi)\cdot\nabla(\psi+z)$ 2D	Richards' equation: $C(\psi)\cdot\frac{\partial\psi}{\partial t} = \frac{\partial}{\partial x}\left(K_{\mathrm{w/s}}(\psi)\cdot\frac{\partial\psi}{\partial x}\right)+\frac{\partial}{\partial z}\left(K_{\mathrm{w/s}}(\psi)\cdot\left(\frac{\partial\psi}{\partial z}+1\right)\right)+S_w$	$S_w = K_{w/s}(\psi)\cdot S_{\mathrm{struc}}\cdot\frac{\psi_{\mathrm{struc}}-\psi}{d^2}$, $\psi_{\mathrm{struc}} = \psi^{ae}\cdot(1-S_{\mathrm{struc}})$
structural	Gravity flow across 7 reservoirs: $q_{struc} = c\cdot S_{struc}{}^{b}, b=1.5$, 1D	for the ith reservoir : $\forall i\in[1..7], V_{\max,i}\frac{dS_{\mathrm{struc},i}}{dt} = (q_{i-1}-q_i)-\int_i S_w(\theta_{mat}, S_{\mathrm{struc},i}, z)$	
crack	instantaneously added at the bottom of the macro-crack,	variation of the depth z^{SL} of the surface of the ponded water according to: **(i)** the flux of water at the surface of the macro-crack, **(ii)** the volume of ponded water that infiltrates horizontally into the soil prism, **(iii)** the swelling of the soil prism,	macro-crack - matric porosity: under the surface of ponded water, Dirichlet boundary condition: $\psi(z\geq z^{\mathrm{SL}}) = z - z^{\mathrm{SL}}$, macro-crack - structural porosity: no exchange

Parameters

matric porosity	hydraulic conductivity $K_{w/s}(\psi)$ retention curve $\psi(\theta)$ shrinkage curve	measured measured measured
structural porosity	c d b ψ^{ae}	unknown: to fit unknown: to fit 1.5 measured: -316 cm

Figure 1:

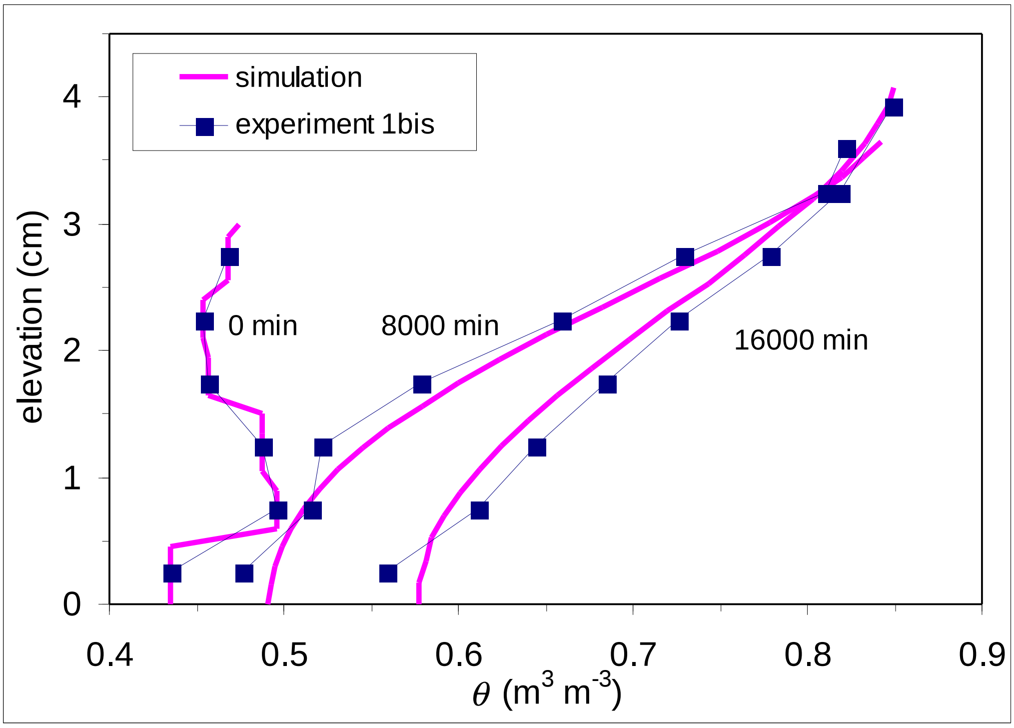
simulation
experiment 1bis
0 min
8000 min
16000 min
elevation (cm)
0
1
2
3
4
0.4
0.5
0.6
0.7
0.8
0.9
θ (m^3 m^{-3})

Figure 2:

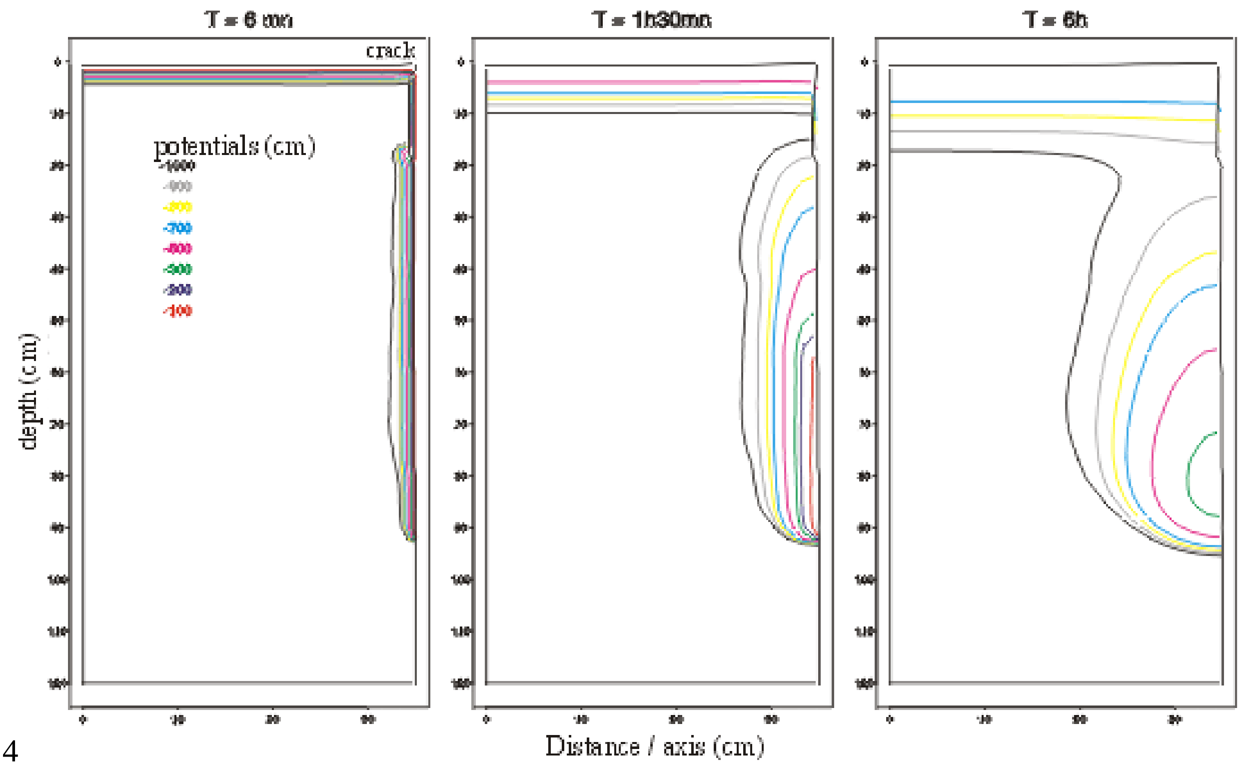
T = 6 mn
T = 1h30mn
T = 6h
crack
potentials (cm)
-700
-100
depth (cm)
Distance / axis (cm)

Figure 3:

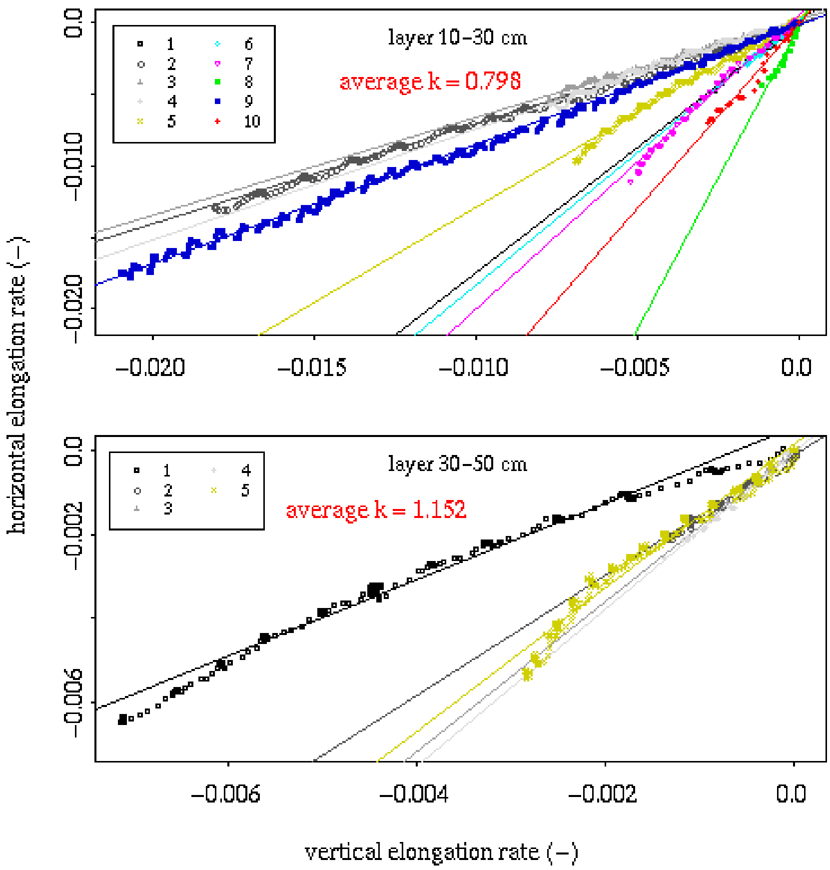
layer 10–30 cm
average k = 0.798
1
2
3
4
5
6
7
8
9
10
layer 30–50 cm
average k = 1.152
horizontal elongation rate (–)
vertical elongation rate (–)
0.0
−0.010
−0.020
−0.020
−0.015
−0.010
−0.005
0.0
−0.002
−0.006
−0.006
−0.004
−0.002

Figure 4

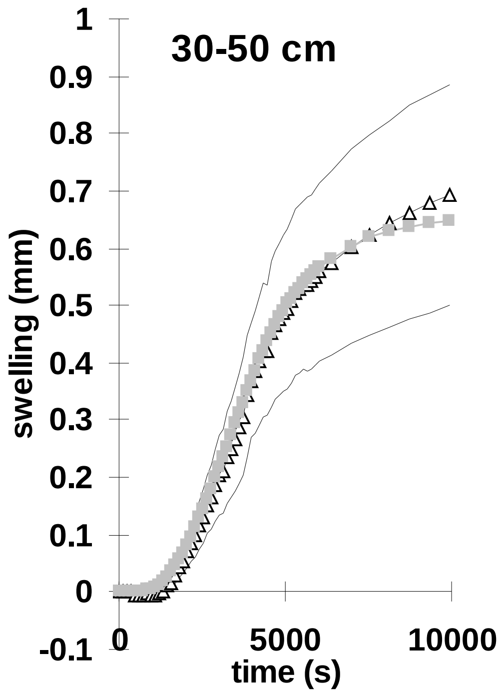
30-50 cm
swelling (mm)
time (s)
1
0.9
0.8
0.7
0.6
0.5
0.4
0.3
0.2
0.1
0
-0.1
0
5000
10000

Figure 5:

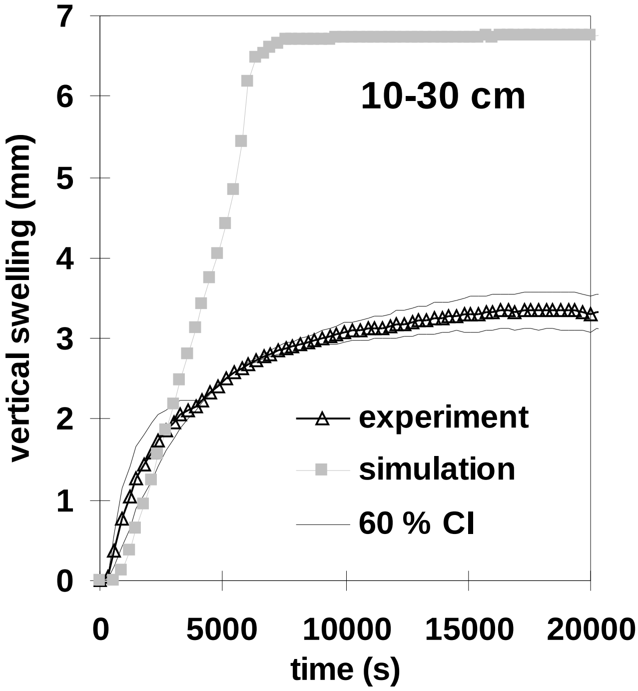

Figure 5a

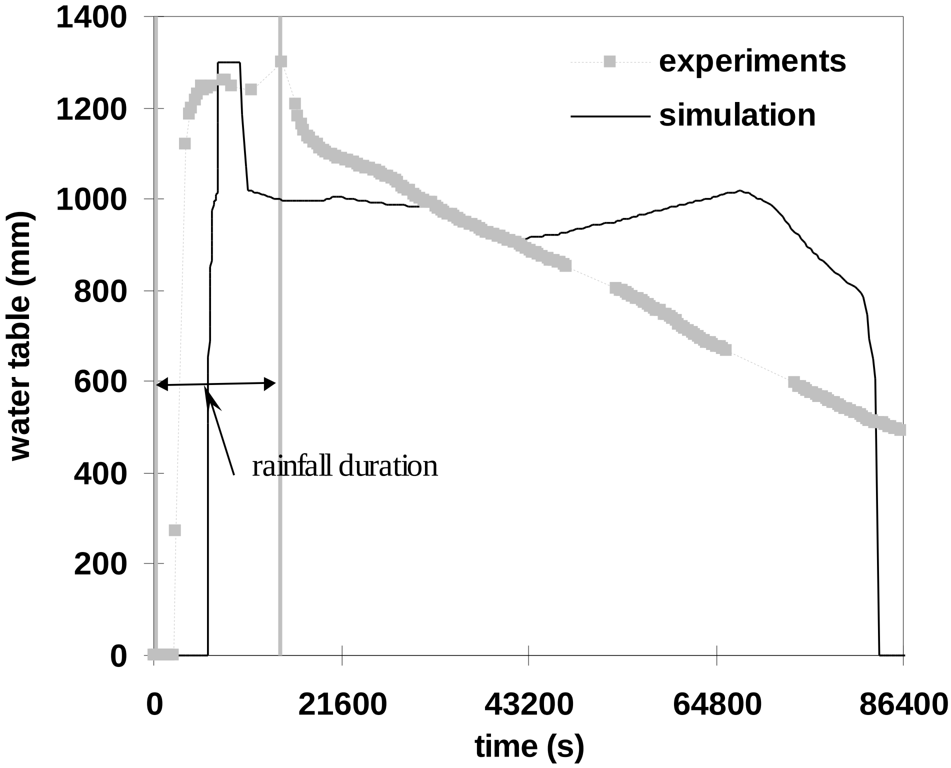

Figure 5b

Figure 6:

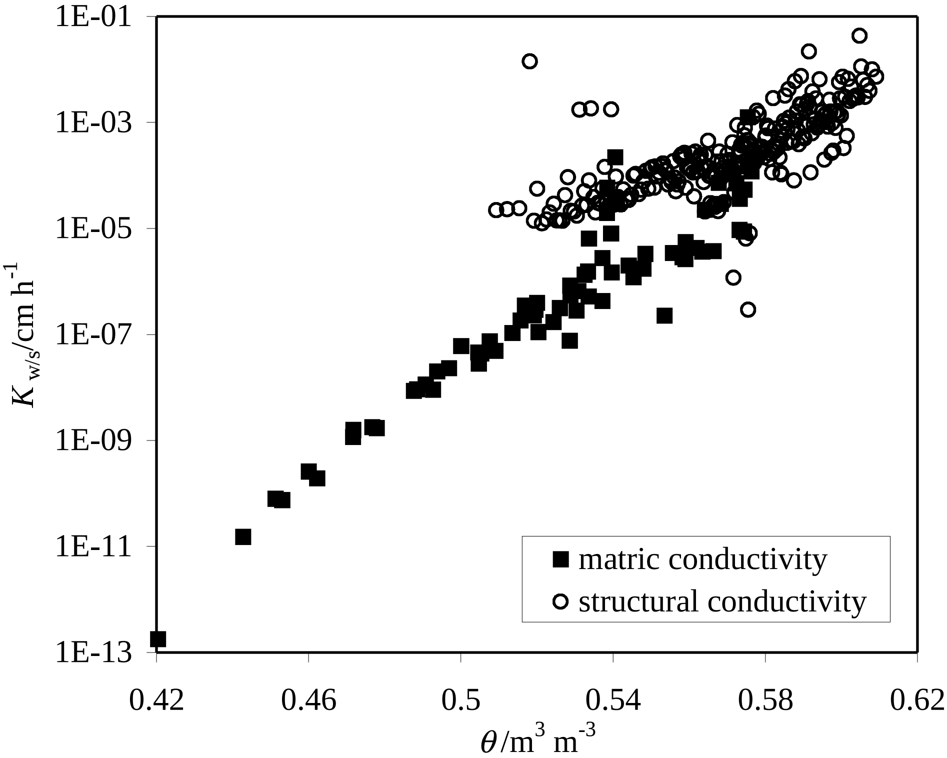
1E-01
1E-03
1E-05
1E-07
1E-09
1E-11
1E-13
$K_{w/s}$/cm h^{-1}
0.42
0.46
0.5
0.54
0.58
0.62
θ/m^3 m^{-3}
matric conductivity
structural conductivity

Figure 7:

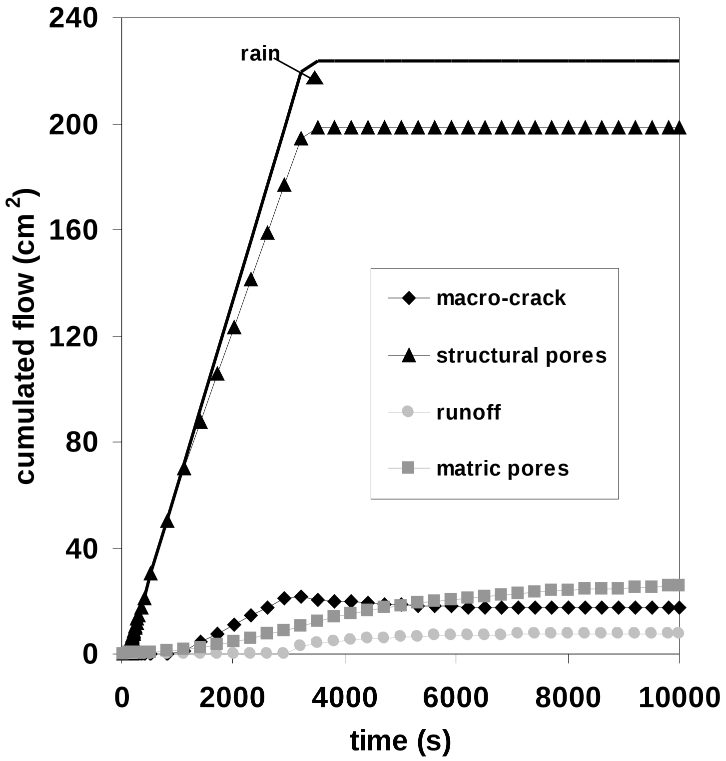

Figure 7a

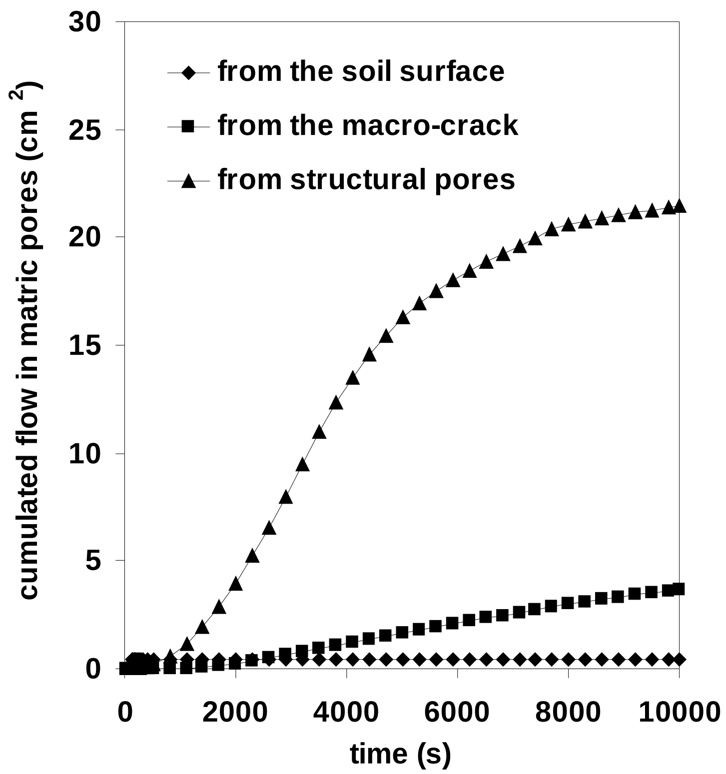

Figure 7b